ELSEVIER

Chemical Engineering Journal 132 (2007) 137–149

Chemical Engineering Journal

www.elsevier.com/locate/cej

Prediction of flow behavior of micro-particles in risers in the presence of van der Waals forces

Shuyan Wang [a], Huilin Lu [a,*], Zhiheng Shen [a], Huanpeng Liu [a], Jacques Bouillard [b]

[a] *School of Energy Science and Engineering, Harbin Institute of Technology, Harbin 150001, China*
[b] *INERIS, Parc Technologique Alata, BP2, Verneuil-en-Halatte 60550, France*

Received 28 July 2006; received in revised form 20 January 2007; accepted 23 January 2007

Abstract

Flow behavior of gas and micro-particles in riser is predicted within the framework of the classical Euler–Lagrange approach. The Newtonian equation of motion considering the effect of van der Waals forces is solved for each simulated particle in the system. Particle collisional dynamics is modeled by means of the direct simulation Monte Carlo (DSMC) method. The influence of van der Waals forces on the particle collisions is investigated. The effect of interparticle collisions on the particle concentration and velocity distributions is presented. These numerical results allow one to understand the effect of the considered parameters on the flow behavior of micro-particles agglomerations.

Keywords: DSMC method; Micro-particles; Interparticle van der Waals forces; Riser

1. Introduction

Micro-particles in which surface forces play an important role in the mechanical behavior of particles are classified to the Geldart group C [1]. Strong cohesive forces between micro-particles promote the fluidization of aggregates of primary particles [2]. Properties of the fluidized aggregates, rather than those of primary particles, determine the hydrodynamic behavior of risers. Experiments indicated that the elutriation rate of group C particles decreased with the increase of the particle mean diameter under the condition of a given superficial gas velocity in the fluidized bed [3]. Sound waves, mechanical vibration, gas pulsation, and magnetic and centrifugal fields have been applied to provide external forces to improve the fluidization of fine particles [4–7]. Experimental results indicated that with assistance of external forces the bed of agglomerates can be readily fluidized, and the flow structures of channeling or slugging disappeared and the bed expanded uniformly.

On the other hand, Mikami et al. [8] simulated the fluidized behavior of cohesive particles using a discrete numerical simulation model considering the effect of liquid bridge force and particle–particle interaction force in a two-dimensional bubbling fluidized bed. Helland et al. [9] simulated the flow structure of cohesive particles in a two-dimensional riser by a hard-sphere discrete particle model. Rhodes et al. [10] analyzed the influence of the magnitude of the cohesive force of particles on fluidization characteristics in terms of the change in the ratio of the minimum bubbling to minimum fluidization velocities by a discrete element method. Kuwagi and Horio [11] investigated the mechanism of agglomeration in a bubbling fluidized bed of cohesive fine particles by a two-dimensional discrete element method. Ye et al. [12] studied the fluidization behavior of Geldart A particles by use of a soft-sphere discrete particle model considering the interparticle van der Waals forces. The particle circulation and bubble flow were predicted in the bubbling fluidized bed.

Turbulent particle agglomeration is an important mechanism especially for micro-particles flow [13]. For such small particles, Brownian motion and gravitational settling generally are negligible compared to turbulence-induced motion. Moreover, van der Waals interaction dominates in fluidized transport system of micro-particles, so that they tend to stick together to form particle aggregates when they collide with each other. The lack of detailed information in the open literature concerning the motion of micro-particles has hindered further investigation of flow behavior of micro-particles in the riser. A better understanding of the flow behavior of micro-particles is therefore of great importance in applications involving mixing and transporting of micro-particles. The purpose of this study is to investigate the effect of van der Waals forces on the flow

* Corresponding author. Tel.: +86 10 045186412258.

1385-8947/$ – see front matter © 2007 Elsevier B.V. All rights reserved.
doi:10.1016/j.cej.2007.01.043

Nomenclature

a_i	local area of a particle i (m^2)
A	Hamaker constant (J)
B	Boltzman's constant (J/K)
c_{do}	drag coefficient
d	particle diameter (m)
D	diameter of riser (m)
e	coefficient of restitution of particles
e_w	coefficient of restitution between particle and wall
f_c	collision frequency of particles (s^{-1})
f_d	drag force (Pa)
F	time fraction (s)
g	gravity ($m\,s^{-2}$)
G_s	solid mass flux ($kg\,m^{-2}\,s^{-1}$)
h	height of riser (m)
$\hbar$	Planck's constant (J s)
$\mathbf{I}$	unit vector
m	particle mass (kg)
n	particle number density
ns	number of real particle/simulated particle
N	refractive index
p	fluid pressure (Pa)
p_{ij}	collisional probability
P_p	material limiting contact pressure (Pa)
r	position, distance from center (m)
R	random number, radii of particle and riser
s	local area of a particle (m^2)
t	time (s)
T	absolute temperature (K)
u_g	gas velocity, superficial gas velocity ($m\,s^{-1}$)
v	particle velocity ($m\,s^{-1}$)
x	location along lateral direction (m)
y	location along vertical direction (m)
z_0	contact distance (m)

Greek symbols

α	dielectric constant
ε_g	porosity
ε_s	solid concentration
θ	granular temperature ($m^2\,s^{-2}$)
$\mu_{lam,g}$	laminar viscosity of gas phase (Pa s)
μ_t	turbulent viscosity of gas (Pa s)
ν_e	absorption frequency (s^{-1})
ρ_g	gas density ($kg\,m^{-3}$)
ρ_s	particle density ($kg\,m^{-3}$)
σ	standard deviation
τ_g	gas stress tensor (Pa)

Subscripts

g	gas phase
i	index of particle
n	normal direction
s	particles

behavior of micro-particles in a riser through DSMC simulation. The distributions of velocity and concentration of particles in the riser are analyzed. It is expected that the results of this study would stimulate further discussion and development of the micro-particle interaction models in risers. This would eventually enable new insights into the mechanism of agglomerate micro-particles in risers to be revealed.

2. Eulerian–Lagrangian gas–solid flow model

2.1. Continuity and momentum equations for gas phase

The Euler–Lagrangian method computes the Navier–Stokes equation for the gas phase and the motion of individual particles by the Newtonian equations of motion. For the gas phase, we write the equations of conservation of mass and momentum [14,15]:

$$\frac{\partial}{\partial t}(\rho_g \varepsilon_g) + \nabla \cdot (\rho_g \varepsilon_g u_g) = 0 \tag{1}$$

$$\frac{\partial}{\partial t}(\varepsilon_g \rho_g u_g) + \nabla \cdot (\varepsilon_g \rho_g u_g u_g) = -\varepsilon_g \nabla P - S_{p-g} - (\varepsilon_g \nabla \cdot \tau_g) + \varepsilon_g \rho_g g \tag{2}$$

where u_g and ρ_g are gas velocity and density, respectively. ε_g is porosity, and S_{p-g} the interaction drag force acting on a particle. The interaction force between the two phases should be equal and has reverse direction. The value can be determined by

$$S_{p-g} = \frac{\sum_{i=1}^{N} a_i f_{d,i}}{\sum_{i=1}^{N} a_i} \tag{3}$$

where a_i is the area of particle i in the cell. The drag force, $f_{d,i}$, is calculated by Eq. (7). The stress tensor of gas phase can be represented as

$$\tau_g = \mu_g[\nabla u_g + (\nabla u_g)^T] - \tfrac{2}{3}\mu_g(\nabla \cdot u_g)\mathbf{I} \tag{4}$$

The gas turbulence is modeled using a simple subgrid scale (SGS) model. The model was first used and proposed by Deardorff [16] for channel turbulence flow. The SGS model simulates the local Reynolds stresses arising from the averaging process over the finite-difference grid by about the crudest of methods, that involve an eddy coefficient with magnitude limited in some way by the size of the averaging domain. This domain is considered to be the grid volume in a detailed numerical integration. Then the eddy coefficient becomes a "subgrid scale" coefficient:

$$\mu_g = \mu_{lam,g} + \rho_g (C_t \Delta)^2 \sqrt{S_g : S_g} \tag{5}$$

where $\Delta = (\Delta x \Delta y)^{1/2}$ and $S_g = (1/2)[\nabla \cdot u_g + \nabla \cdot u_g^T]$. Deardorff suggested C_t be in the range of 0.1–0.2 [16]. In this study $C_t = 0.1$ was used in the simulations.

2.2. Particle motion equations

The particle motion is subject to Newton's equation of motion. Basset, Magnus and Saffman forces should not be included in the Newtonian equations of motion anyway since

they are not real physical forces. Only contact, buoyant, interparticle and gravitational forces enter in the Newtonian force balance. The equation of translational motion of a particle can be written as follows [17,18]:

$$m_i \frac{\mathrm{d}v_i}{\mathrm{d}t} = -\frac{\pi}{6} d_i^3 \nabla p + m_i g + f_{\mathrm{d},i} + F_{\mathrm{v},i} \tag{6}$$

where m_i and v_i represent the mass and velocity of a particle. The first term of the right-hand side of Eq. (6) represents the effects of gas pressure gradients, the second term gravity, the third term the drag force caused by the gas phase, and the last term cohesive force [12,17]:

$$f_{\mathrm{d},i} = \frac{1}{16} c_{\mathrm{d}0,i} \rho_{\mathrm{g}} \pi d_i^2 |u_{\mathrm{g}i} - v_i| (u_{\mathrm{g}i} - v_i) \varepsilon_{\mathrm{g}}^{-\delta} \tag{7}$$

where the drag force coefficient $c_{\mathrm{d}0,i}$ is written as

$$c_{\mathrm{d}0,i} = \left(0.63 + \frac{4.8}{\mathrm{Re}_{\mathrm{p},i}^{0.5}}\right)^2 \tag{8}$$

$$\mathrm{Re}_{\mathrm{p},i} = \frac{\rho_{\mathrm{g}} d_i |u_{\mathrm{g}i} - v_i|}{\mu_{\mathrm{g}}} \tag{9}$$

$$\delta = 3.7 - 0.65 \exp\left[\frac{-(1.5 - \log_{10} \mathrm{Re}_{\mathrm{p},i})^2}{2}\right] \tag{10}$$

For molecules, the van der Waals force arises as a consequence of charge interactions between molecules, which includes dipole–dipole, dipole-induced dipole, and dispersion forces [19]. When applied to two spherical particles that contain many molecules at the surface, it can be determined as [12]:

$$F_{\mathrm{v},i} = \frac{A d_i}{24 s^2} \tag{11}$$

where A is the so-called Hamaker constant that is related to material properties. Note that Eq. (11) exhibits an apparent numerical singularity if the intersurface distance s between two particles approaches zero. This unrealistic singularity incurred at particle contact is avoided by introducing a "cutoff" distance, s_{cut}. In the present model, a minimum cutoff distance of 4×10^{-10} m (40 nm) is used, which is based on the average interatomic distance for many common solids [20,21].

The two-dimensional porosity in a computational cell is the ratio of the surface occupied by the gas to the surface of the computational cell ($\Delta x \Delta y$). If a_i is the surface of simulated particle i inside a computational cell, the porosity in this cell is

$$\varepsilon_{\mathrm{g,2D}} = 1 - \sum_{i=1}^{N} \frac{a_i}{\Delta x \Delta y} \tag{12}$$

The porosity calculated in this way is based on a two-dimensional analysis, which is inconsistent with the applied empiricism in the calculation of the drag force exerted on a particle. Therefore, we utilize a pseudo-three-dimensional concept in which we assume the depth of the cell equal to the particle diameter. The porosity is calculated as follows [17,18]:

$$\varepsilon_{\mathrm{g,3D}} = 1 - \tfrac{2}{3}(1 - \varepsilon_{\mathrm{g,2D}}) \tag{13}$$

Thus, the porosity estimation was corrected in order to use subsequently obtain a representative drag force estimate in three-dimensional (3D) analysis.

2.3. Agglomeration model

The DSMC method is a trajectory method which makes it possible to deal with interparticle collision based on sample particles that the number of which is smaller than the actual number of particles [22]. In the DSMC, a sample particle motion is decoupled from the gas motion by applied external force and collision processes. The motion of these simulated particles obeys the single particle motion model, while the collision process follows the particle collisional dynamics [23,24]. The DSMC method used in this study is described in detail in Shuyan et al [25].

An agglomerate should be defined as a group of particles connected by contact points which can be exist even when forces other than cohesion and repulsion are removed. Iwadate and Horio [26] proposed the following criterion: if $F_{\mathrm{rep;max}} > F_{\mathrm{coh}}$, a pair of particles in a particular contact point are separated after collision. Otherwise, two particles will be agglomerated after collision, where $F_{\mathrm{rep;max}}$ is the maximum repulsion force, and F_{coh} is the maximum cohesion force by van der Waals force.

When two particles collide, they may be separated or agglomerated after collision. The fundamental criterion that determines whether two particles will agglomerate is related with the critical velocity v_{cr}, which is calculated from an energy balance. When only the van der Waals force is considered the critical velocity v_{cr} is given by [13]:

$$v_{\mathrm{cr}} = \frac{1}{d} \frac{(1 - e^2)^{1/2}}{e^2} \frac{A}{\pi z_0^2 \sqrt{9 P_{\mathrm{p}} \rho_{\mathrm{s}}}} \tag{14}$$

where e is the restitution coefficient of particles, z_0 the contact distance, and P_{p} is the material limiting contact pressure. The formation of an agglomerate from two colliding particles takes place when the normal relative velocity between them is less than the critical velocity v_{cr}:

$$|v_i - v_j| \cos\phi \leq v_{\mathrm{cr}} \tag{15}$$

where ϕ is angle between two incident particle trajectories at the collision point. If the condition (15) is valid (i.e. collision), we assumed that two colliding particles have the same velocity and flow direction. This implies that they will move together. Hence, two colliding particles have the following velocity [27]:

$$v_{i,1} = v_{i,0} - \tfrac{1}{2} v_{ij} \quad \text{and} \quad v_{j,1} = v_{j,0} + \tfrac{1}{2} v_{ij} \tag{16}$$

Thus $v_{i,1} = v_{j,1}$. This implies that the relative velocity of the two particles after collision, $v_{ij,1}$, is zero. The energy loss due to the particle collision is $m(v_{ij}^2 - v_{ij,1}^2)/4 = m v_{ij}^2/4$. This is, of course, only the first approach in modeling agglomeration. In further studies, the evolving diameter and density of the agglomerate will be modeled so that the diameter and density of the agglomerate would increase accordingly. If the condition (15) is not valid, two particles will be separated after collisions.

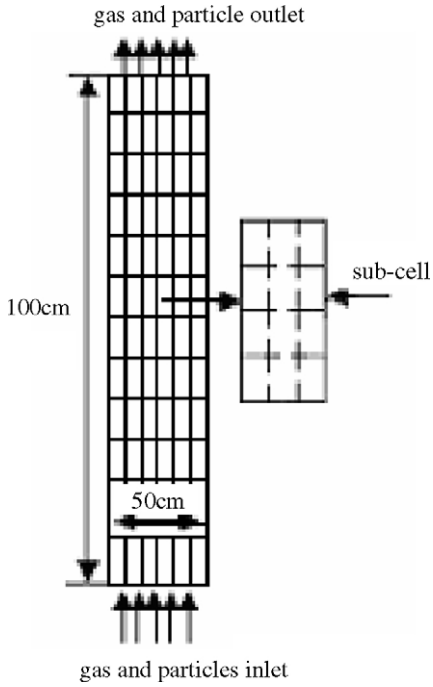

Fig. 1. Grid arrangement in the two-dimensional riser.

2.4. Initial and boundary conditions

Fig. 1 shows the two-dimensional riser section used in the present numerical simulation of gas–solids flow. Initially, the velocities of gas and particles phases were set at zero in the riser. Inlet gas pressure, gas velocity and particle velocity are given. Uniform bottom-inlet condition is assumed. A no-slip condition is used for gas phase at the walls. The particle velocity after it rebounds from the wall can be determined by

$$v_{i2} = -e_w(v_{i1}) \quad (17)$$

where e_w is a restitution coefficient between particle and wall.

In order to efficiently improve the computer capacity to perform the simulations, the sub-cell method described in [22,25] is applied. The computing field is divided into several gas cells. A gas control cell is also divided into several sub-cells, seeing Fig. 1. The search for a collision partner is carried out in the sub-cells, and the interaction between gas and particle phases is calculated in a gas control cell. With this method the collision partner can be more efficiently determined.

The simulations were carried out with a modified CFD code named K-FIX, which was previously used to model the two-phase flows in a circulating fluidized bed [28,29]. Eqs. (1) and (2) were solved based on a finite volume method. The SIMPLE scheme was used as an iterative solution procedure [30]. All present simulations were continued for 10.0 s of real modeling time. Time-average results were obtained over a period lasting 6.0 s. The computation time for one case simulation is about 1–2 weeks on a PC with 80 GB hard disk space, 128 Mb RAM and 600 MHz CPU.

3. Result and discussions

3.1. Basic case simulations

In the base simulations, the diameter and density of particles, and inlet gas velocity were set to be 1.0 μm, 1600 kg m^{-3} and 46.0 cm/s, except otherwise specified. The parameters used in the simulations were listed in Table 1.

Fig. 2 shows a snapshot of simulation representing vertical cross-section images as a function of times. The formation, movement and breaking of agglomerates are observed at locations of high particle concentrations. The agglomerates exhibits shapes of stick-figures, V-type shapes heading upwards or downwards, circles and others irregular shapes in the riser.

Fig. 3 shows the instantaneous particle concentrations near the wall ($r/D = 0.475$) and at the center ($r/D = 0.025$) of riser, respectively. High solids concentrations in computational cells mean the existence of agglomerates. Comparing with particles flow at the center regime, there are more oscillations near the walls. Fig. 4 shows the distribution of time-averaged concentration of particles at the different heights. The particle concentration decreases along the height. The core-annulus structure of micro-particles flow can be observed with a denser zone close to the walls and a dilute zone in the center. The distributions of time-averaged velocity of particles are shown in Fig. 5 at the different heights. The time-averaged axial velocity of particles is lower near the walls than that at the center. In the center, particles flow up at high velocity and low concentration, and at low velocity and high concentration near the walls. Comparing Fig. 5a and b, it can be seen that the axial velocity of particles is much larger than that the lateral velocity of particles because particles are mainly flowing up in the riser.

The histograms of axial and lateral particle velocities are shown in Figs. 6 and 7. The mean values of particle veloc-

Table 1
Parameters used in simulations

Particle diameter (μm)	1.0	Inlet particle flux number (s^{-1})	1,000,000
Particle density (kg m^{-3})	1600	Particle restitution coefficient	0.6
Number of real particle/simulated particle	100	Particle–wall restitution coefficient	0.6
Height of riser (mm)	1000	Diameter of riser (mm)	50
Hamaker constant (J)	1.0×10^{-19}	Particle inter-contact distance (nm)	0.4
Gas viscosity (Pa s)	1.5×10^{-5}	Grid number (nx, ny)	40, 150
Superficial gas velocity (cm/s)	46	Gas density (kg m^{-3})	1.2
CFD time step (s)	1.0×10^{-5}	Limiting contact pressure (Pa)	5.0×10^{9}
Particle dynamics time step (s)	1.0×10^{-7}	Gas temperature (K)	300

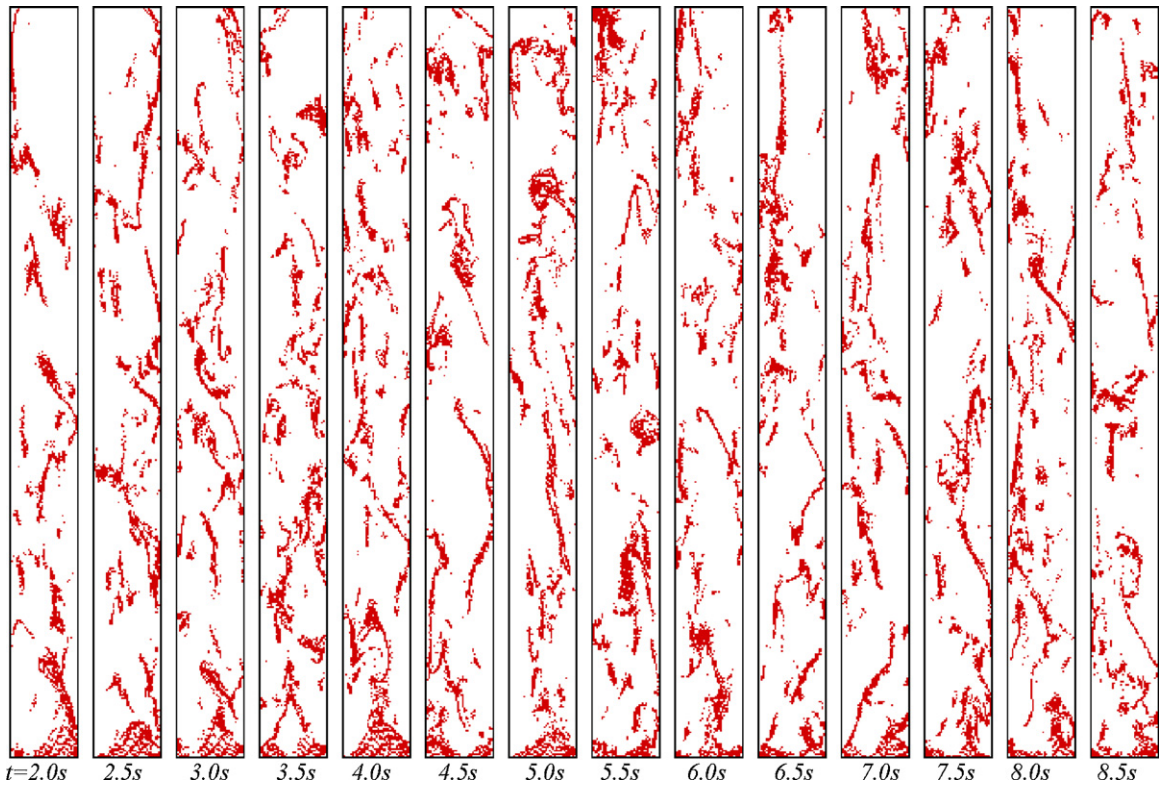

Fig. 2. Instantaneous particles concentration of micro-particles in the riser.

ity and standard deviation, $\sigma = \sqrt{(1/(N-1))\sum_{i=1}^{N}(v_i - v_m)^2}$, are also indicated in the figures, where v_m is a mean velocity, v_i is a instantaneous velocity of particles. The axial and lateral velocities of particles can be fitted by the Gaussian distribution function. Fig. 8 shows the standard deviation of particle velocity as a function of time-averaged concentration of particles. The computed standard deviations of vertical velocity are always larger than that of lateral velocity of particles. The standard deviations are increased with the increase of concentration, reached a maxima, and then decreased. The granular temperature, θ, defined as a measure of particle fluctuations can be calculated from the standard deviations of velocity of particles [31]:

$$\theta = (\tfrac{1}{3}\sigma_y^2 + \tfrac{2}{3}\sigma_x^2) \tag{18}$$

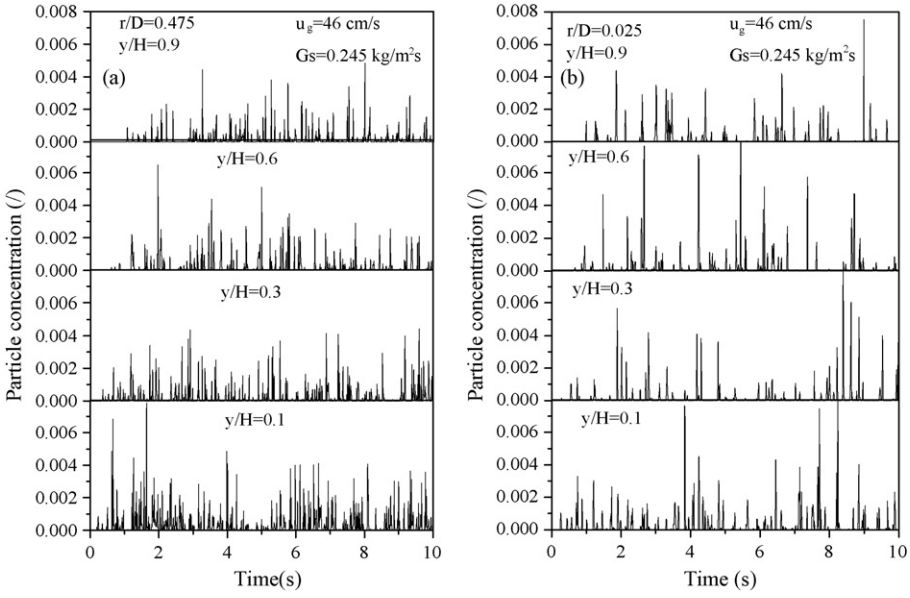

Fig. 3. Instantaneous particle concentration at the different positions in the riser.

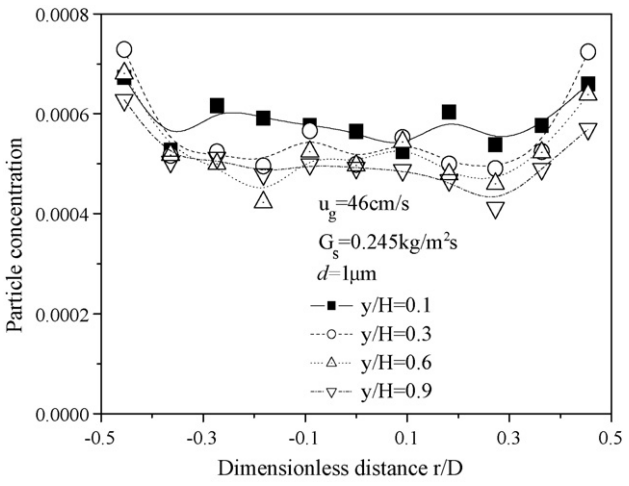

Fig. 4. Distribution of time-averaged particle concentrations.

where σ_y and σ_x are vertical and lateral standard deviations. Fig. 9 shows the computed granular temperature as a function of particle concentration in the riser. The computed granular temperature increases, reaches a maxima, and then decreases with the increase of particle concentration. At the high concentration of particles, the granular temperature decreases due to particle agglomeration. The granular temperature approaches to zero as the concentration of particles goes to zero because of the lack of particle collisions.

Using DSMC method, the collisional frequency of particles was obtained, seeing Fig. 10. The computed collisional frequency increases at low concentration of particles, reaches a maxima, and then decreases with the increase of concentration of particles. The lower the particle concentrations, the less the collisional frequency of particles. However, at the high concentration the collisional frequency decreases because of particle agglomerate effect. Based on the kinetic theory of granular flow, the collisional frequency per unit volume can be calculated as follows [14]:

$$f_c = 6.77 \left(\frac{\varepsilon_s}{d}\right) g_0 \sqrt{\theta} \tag{19}$$

Based on the computed granular temperature and particle concentration in Fig. 9, the collisional frequency of particles calculated from Eq. (19) is also shown in Fig. 10. It can be seen that at the low concentration of particles the calculated collisional frequencies by means of DSMC agree with results calculated by Eq. (19). However, there is a large difference between them at the high concentration of particles. The collisional frequency calculated from Eq. (19) is higher than that directly from DSMC. The most probable reason could be that at high concentrations most particles were formed into the collected agglomerates flow, not dispersed flow that assumed in the derivation of Eq. (19) in kinetic theory of granular flow [14]. Hence, to gain more insight into the effect of agglomeration of particles on the collisional behavior, it seems worthwhile to

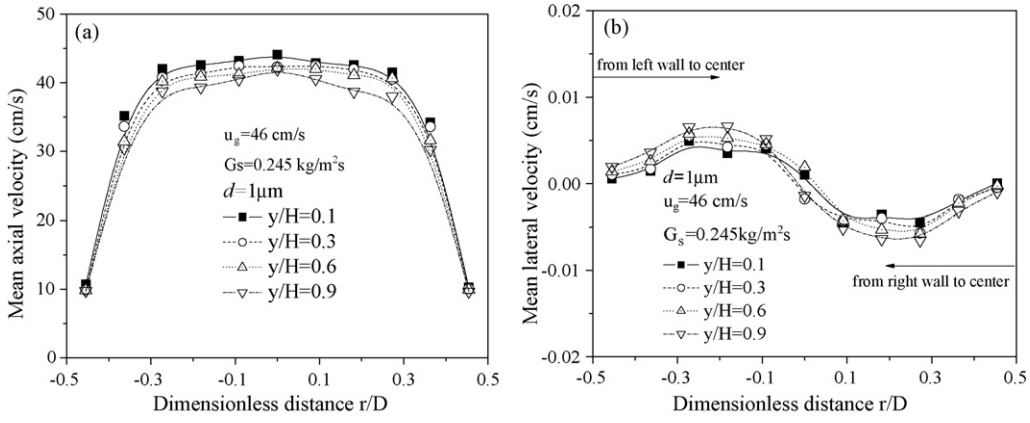

Fig. 5. Distributions of time-averaged axial and lateral velocity of particles.

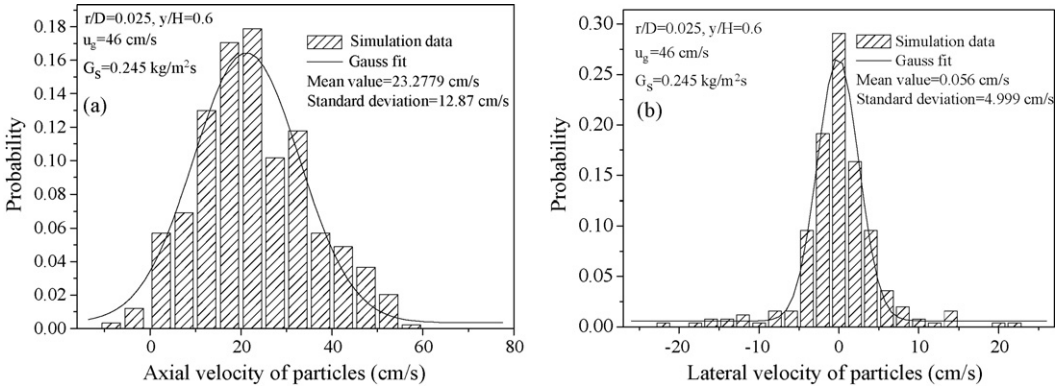

Fig. 6. Distribution of transversal and axial velocity of particle near the center.

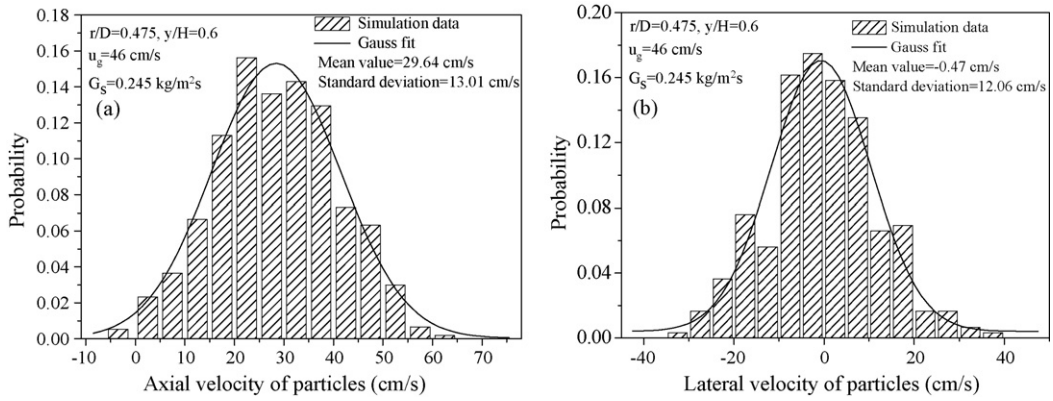

Fig. 7. Distribution of transversal and axial velocity of particle near the wall.

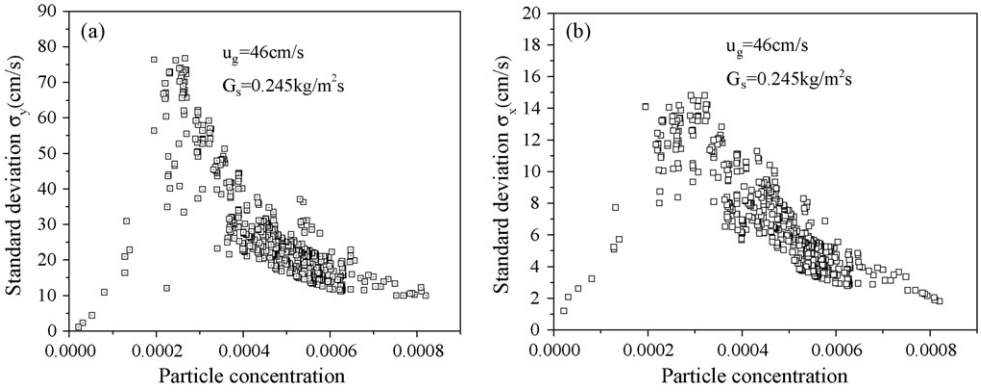

Fig. 8. Distribution of standard deviation of particles as a function of concentration of particles.

modify the present kinetic theory of granular flow considering particle agglomerate effect, which will be a subject of future research.

A typical distribution of the instantaneous positions and vertical velocities of the simulated particle, and particle concentration in a computational cell is shown in Fig. 11. The velocity of the simulated particle changes as it is captured by an agglomerate or escapes from an agglomerate. At the AB phase in Fig. 11a, the vertical velocity of the simulated particle is reduced, and the concentration of particles of the computational cell is increased. This means the simulated particle is captured by agglomerate. While the concentration of particles in the computational cell drops, and the vertical velocity of the simulated particle is increased at the BC phase. This indicates the simulated particle is escaped from agglomerate. A single micro-particle will have a high velocity due to the effect of high velocity of gas phase. At the CD phase the concentration of particles in the computational cell is very low, and the vertical velocity of simulated particle is high. This is a feature characterizing particle dispersed in dilute flow. The simulated particle was decelerated when it was captured

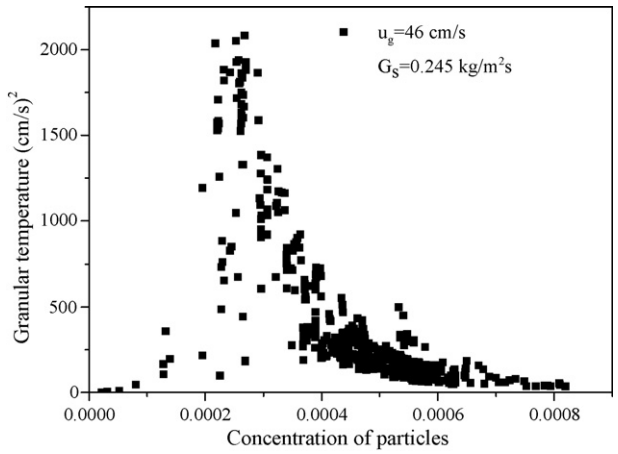

Fig. 9. Relation between granular temperature and particle concentrations.

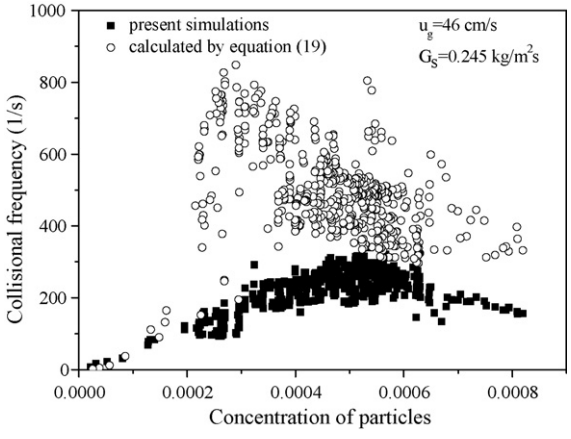

Fig. 10. Profiles of particle collision frequency as a function of concentration of particles.

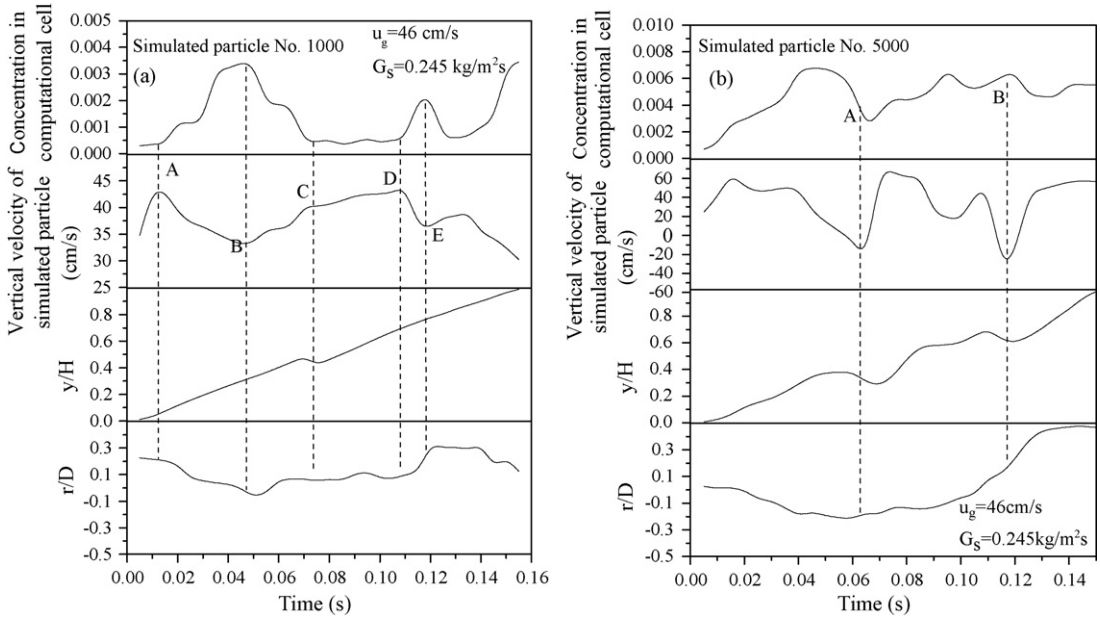

Fig. 11. Instantaneous positions, and vertical velocity of simulated particle and particle concentration of gird.

by agglomerate, and re-accelerated when it left from the agglomerate. Hence, the life of an agglomerate can be described by three periods: a formation phase, an established phase and a decaying phase. During the agglomerate formation, like at the AB and DE phases in Fig. 11a, particles are decelerated and simultaneously, the gas phase is accelerated due to the two-way coupling between the gas and particle phase, thus increases in their relative velocity. The concentration of particles in the computational cell was also increased. In the established phase, like at the point B in Fig. 11a, the velocity of the agglomerate as a unit is found to be constant. The concentration of particles in the computational cell is invariable. In the decaying stage at the BC phase in Fig. 11a, the agglomerate may take a part of an new agglomerate, or break into dispersed single particles, and the velocity was increased and the concentration of particles in the computational cell was reduced. On the other hand, the simulated particle may be trapped into the agglomerate after it enters the riser. Complex transitory velocity and concentration fields are evident from Fig. 4b. High solids concentration in computational cell implies large size of agglomerates. The down-flow of agglomerates is represented by the points A and B in Fig. 11b. The size of agglomerate is varied during it passes through the riser. This suggests that there is a large fluctuation of velocity and concentration of particles in riser due to the formation and breakage of agglomerates.

To obtain quantitative characterization of agglomerate flow in a riser, one first needs a systematic criterion for identification of agglomerates. For particle cluster flow in riser, Sharma et al. [32] proposed the following three necessary guidelines: (1) the solid concentration in a particle cluster must be significantly above the time-average solid concentration at the given local position and operating condition. (2) This perturbation in solid concentration due to particle clusters must be greater than the random background fluctuations of particle concentration. (3) This concentration perturbation should be sensed for sampling volume with characteristic length scale greater than one to two orders of particle diameter. These guidelines were used in the determination of cluster flow of FCC particles in the riser [25]. In the present analysis, we will use these criteria in that the local instantaneous particle concentration for an agglomerate must be greater than the time-averaged concentration by at least one time the standard deviation σ, as shown in Fig. 12. An agglomerate would thus be identified if the instantaneous particle concentration exceeds this threshold, existing until the particle concentration again drops below this threshold. We would like to point out here that the agglomerate detection criterion described above is reasonable, but also is somewhat arbitrary. Using a different factor to differentiate from background noise, e.g. 2σ, would alter the quantitative results to some degree, but would not change the general characteristics of agglomerate dynamics. The agglomerate duration time is

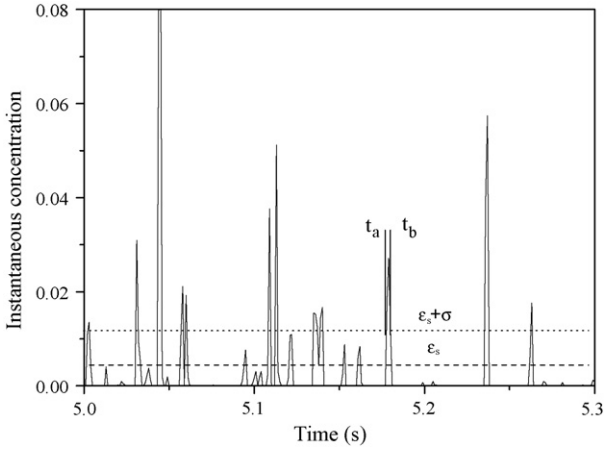

Fig. 12. Determination of an agglomerate formation.

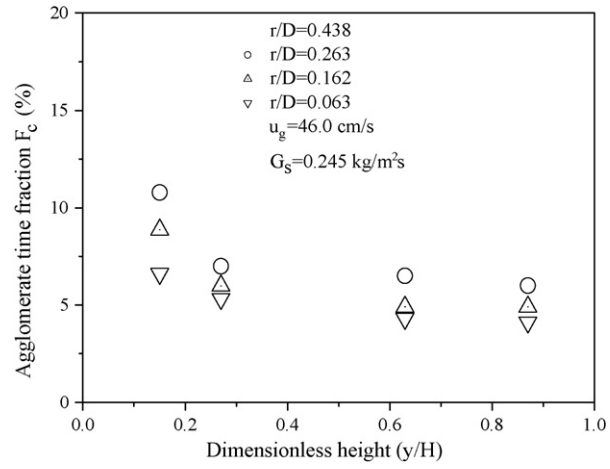

Fig. 13. Time fraction of agglomerates with bed height.

$\tau_c = t_b - t_a$. The number-averaged duration time is then

$$\bar{\tau}_c = \sum_{i=1}^{n} \frac{\tau_{ci}}{n} \tag{20}$$

where n is the total number of agglomerates detected in an simulation period. τ_{ci} is the ith agglomerate's duration time. The agglomerate existence time fraction F_c is

$$F_c = \frac{\bar{\tau}_c}{\tau} \tag{21}$$

where τ is the simulation time within which n agglomerates are detected. So the agglomerate occurrence frequency λ_c can be obtained. Fig. 13 shows the distribution of agglomerate existence time fraction along the height. The existence time fraction of agglomerates decreases along the height at the center. But near the walls it is almost constant. This means that agglomerates are easily formed at the bottom. The existence time fraction of agglomerates is greater at the wall region than that in the center. Fig. 14 shows the agglomerate occurrence frequency at the superficial gas velocity and solid mass flux of

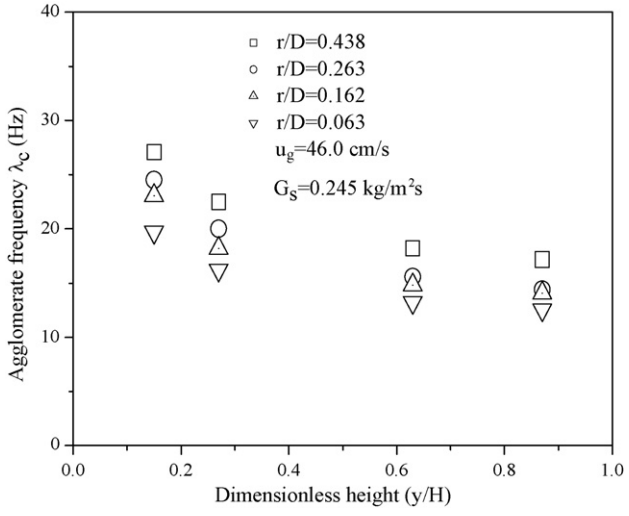

Fig. 14. Agglomerate frequency along bed height at the superficial gas velocity of 46 cm/s.

46.0 cm/s and 0.245 kg m^{-2} s^{-1}, respectively. The agglomerate occurrence frequency (or time fraction of agglomerate life) is greater near the walls than that at the center. The agglomerate occurrence frequency increases at the bottom due to the inlet effect. The occurrence frequency is nearly constant at the top of riser. We see that the simulated occurrence frequency of agglomerate is about 16–27 (Hz).

3.2. Comparison with experimental data of Li et al. [33]

Li et al. [33] measured particle concentrations obtained from the measurements of pressure drop distribution along height in a riser. The riser is a 3.25 m in height, 75 mm in internal diameter glass tube. Above the gas distributor there are 15 probe taps along the riser at 0.2 m intervals. The surface modified (coated with a thin-film of stearic acid) cubic-lattice $CaCO_3$ (MCC) particles was used. The diameter and density of $CaCO_3$ (MCC) particles are 4.3 μm and 2539 kg m^{-3}, respectively. A detailed description of the unit can be found in Li et al. [33]. The Hamaker constant A accounts for the material properties and is independent of the system geometry and the separation distance [34]. Israelachvili [35] showed that using the Lifshitz continuum approximation of the van der Waals force [36], the Hamaker constant for the solids (a) interacting through a medium (b) can be expressed as follows:

$$A = \frac{3}{4}BT\left[\frac{\alpha_a - \alpha_b}{\alpha_a + \alpha_b}\right]^2 + \frac{3\hbar\nu_e}{16\sqrt{2}}\frac{(N_a^2 - N_b^2)^2}{(N_a^2 + N_b^2)^{3/2}} \tag{22}$$

where B is the Boltzman's constant (=1.381 × 10^{-23} J/K), $\hbar$ the Planck's constant (=6.626 × 10^{-34} J s) and ν_e is the absorption frequency in the ultraviolet–visible (UV) range. α and N are dielectric constant and refractive index of particles, respectively. The first term in Eq. (22) is the zero frequency term and consists of the Debye and Keesom contribution to the van der Waals force, and the second term is the frequency dependent term and accounts for the London dispersion interactions [35,36]. Hence, the Hamaker constant of $CaCO_3$ particles can be estimated. In what follows, we take the value $A = 1.198 \times 10^{-19}$ J. Gas–particle properties and other related information are listed in Table 2.

Fig. 15 compares the computed axial profile of particle concentrations with experimental data of Li et al. [33] at superficial gas velocities of 1.89 m/s. Both simulated and measured concentration profiles show that the characteristic of high concentration zone is near the inlet due to particle acceleration, and low concentration is at the upper part of riser. For two different coefficients of restitution of particles, the computed concentrations of particles have the same trends along the height of riser. However, for the higher coefficient of restitution, a more uniform distribution of particles is obtained. We see that the simulated concentration of particles is lower at the bottom regime than that of experimental data. Li et al. [33] found that the agglomerates at the bottom are 10–20 times as large as those at the top. These larger agglomerates would lead to deposition at the bottom of riser, while the small agglomerates would flow up to the top of the riser. From images, we can see that particles rapidly formed

Table 2
Parameters used for simulations of Li et al. [33] experiments

Height of riser (m)	3.25	Diameter of riser (cm)	75.0
Diameter of inlet particles (μm)	4.3	Density of particles (kg m^{-3})	2539
Number of real particle/simulated particle	100	Particle–wall restitution coefficient	0.5
Hamaker constant (J)	1.198×10^{-19}	Particle inter-contact distance (m)	4.0×10^{-10}
Superficial gas velocity (m/s)	1.89	Particle restitution coefficient	0.5
Inlet particle flux (s^{-1})	1,000,000	Inlet solid mass flux (kg m^{-2} s^{-1})	1.229
Dielectric constant of particles	6.14	Refractive index of particles	1.545
Absorption frequency (s^{-1})	3.0×10^{15}	Planck's constant (J s)	6.626×10^{-34}
Gas temperature (K)	300	Limiting contact pressure (Pa)	5.0×10^{9}

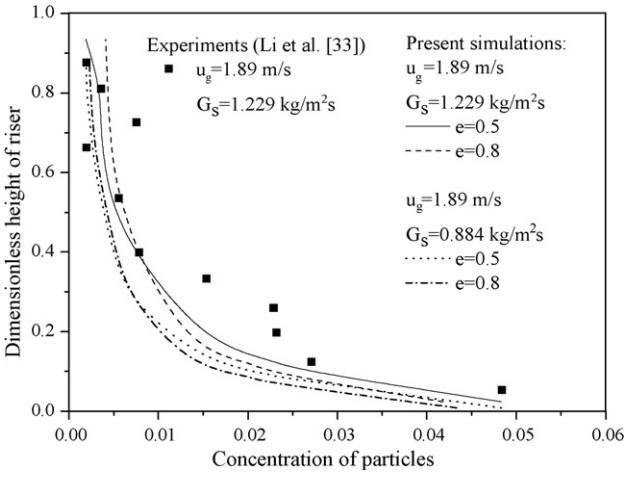

Fig. 15. Computed and experimental concentration of particles at the superficial gas velocity of 1.89 m/s.

into agglomerates in the inlet regime, and then these agglomerates are degraded by the effect of collisions and the interaction of gas phase, or are further congregated by the cohesion of other particles when it passes through the riser.

Fig. 16 shows the existence time fraction of agglomerates of $CaCO_3$ particles along the height at the superficial gas velocity of 1.89 m/s. The effect of coefficient of restitution of particles on the existence time fraction is also shown in this figure. The high coefficient of restitution gives the low existence time fraction of agglomerates because of less energy loss during collisions. The existence time fraction of agglomerates decreases along the height. This means that agglomerates are easily formed at the bottom of riser.

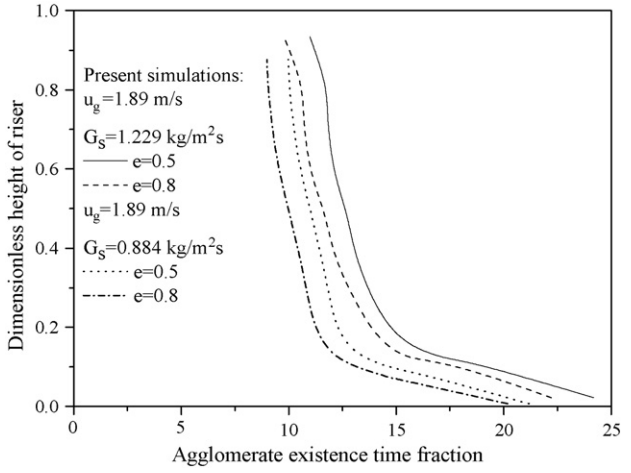

Fig. 16. Profile of agglomerate time fraction at the superficial gas velocity of 1.89 m/s.

3.3. The effect of interparticle van der Waals force

Cohesive forces are known to be a continuous function of particle separation distance, and may result in enduring particle contacts. Hence, the nature of cohesive forces conflicts with the assumption of binary, instantaneous interactions inherent in kinetic theory (continuum) descriptions of granular flows. In this investigation, we carried out for two test cases: the first with a Hamaker constant equals to 1.0×10^{-19} J and the second with a Hamaker constant of 1.0×10^{-18} J (factor of 10 greater). Fig. 17 shows the effect of Hamaker constants on the distribution of velocity of particles at the superficial gas velocity and solid mass flux of 46.0 cm/s and 0.45 kg m^{-2} s^{-1}, respectively. At the Hamaker constant of 1.0×10^{-19} J, the concentration of particles increases toward walls. The concentration of particles was lower in the center than that at walls. However, as the value of Hamaker constant increases from 1.0×10^{-19} to 1.0×10^{-18} J, the opposite behavior is observed. The concentration of particles decreases toward the walls. This seems to imply that the cohesive interactions between particles influence on the distribution of concentration of particles. In case of relatively strong cohesive forces, obvious agglomerates flow have been identified, even at a high gas velocity.

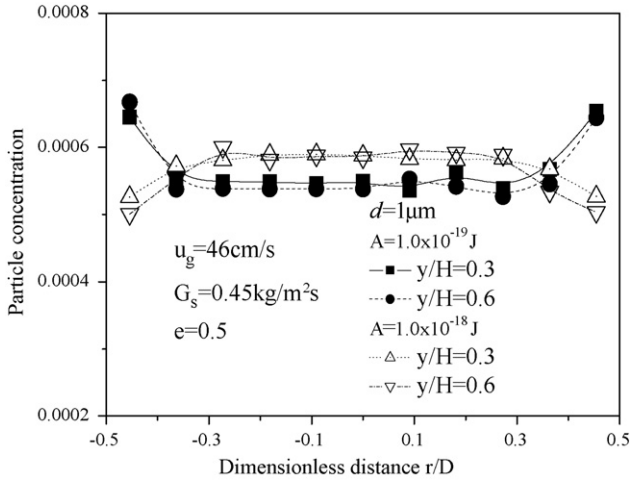

Fig. 17. Distribution of particle concentration with different Hamaker constants.

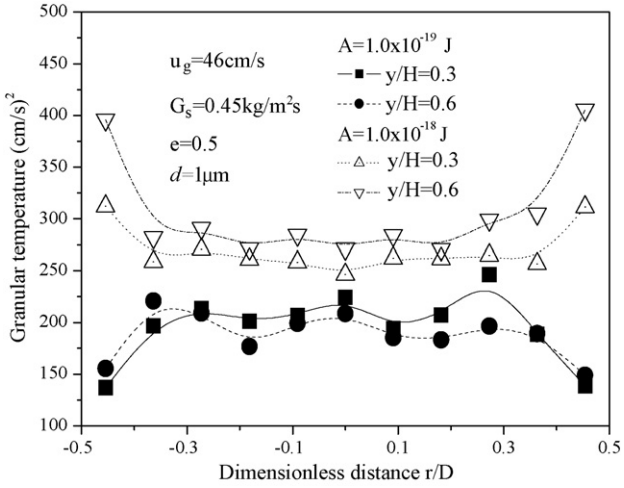

Fig. 18. Profile of granular temperature of with different Hamaker constants.

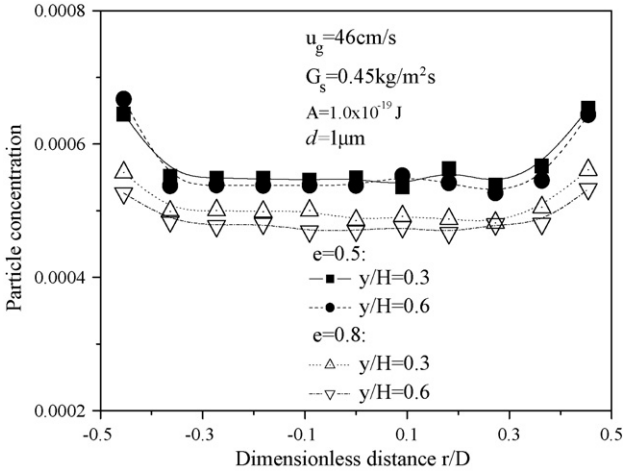

Fig. 20. Distribution of particle concentration with different collisional parameters.

Fig. 18 shows the profiles of granular temperature of particles for two different Hamaker constants at the superficial gas velocity and solid mass flux of 46.0 cm/s and 0.45 kg m^{-2} s^{-1}, respectively. For small Hamaker constant, the granular temperature decreases toward the walls. However, as the Hamaker constant increases from 1×10^{-19} to 1×10^{-18} J the granular temperature increases toward the walls. This indicated that the stronger the cohesional interparticle van der Waals force, the higher the fluctuating velocity. So on the basis of our discrete particle simulations, we conclude that the particle agglomerate is due to both the particle collision and the cohesional interparticle van der Waals dynamic forces.

Fig. 19 shows the distribution of agglomerate frequency at two different Hamaker constants at the superficial gas velocity and solid mass flux of 46.0 cm/s and 0.45 kg m^{-2} s^{-1}, respectively. With the increase of Hamaker constants, the agglomerate frequency was increased. At the Hamaker constant of 1.0×10^{-19} J, the frequency of agglomerates is increased from center toward the walls. However, as the Hamaker constant increases from 1.0×10^{-19} to 1.0×10^{-18} J, the life-time frequency of agglomerates is decreased toward the walls at the same riser height. This indicated that the agglomerates are more easily formed with an increase of Hamaker constant. Simulated results indicated that the life-time frequency of agglomerates decreased along riser height. At least three basic interactions, i.e. the fluid–particle interaction, the particle–particle collisions (and the particle–wall collisions), and the interparticle van der Waals forces, can be identified as the main sources of velocity fluctuations of particles in present study.

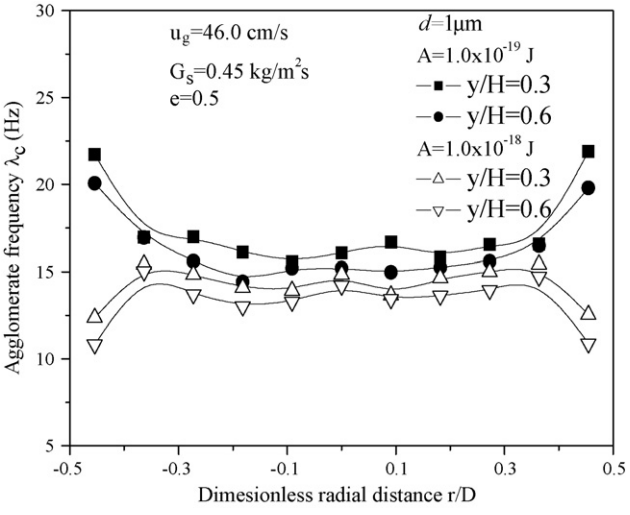

Fig. 19. Agglomerate frequency along bed height with different Hamaker constants.

3.4. Influence of the restitution coefficient on flow behavior of agglomerates

In this investigation, we carried out for two test cases: the first with a restitution coefficient equals to 0.5 and the second with a restitution coefficient is to be 0.80 (60% increase). Fig. 20 represents the distribution of particle concentration in the riser at the superficial gas velocity and solid mass flux of 46.0 cm/s and 0.45 kg m^{-2} s^{-1}, respectively. We observed that at a low

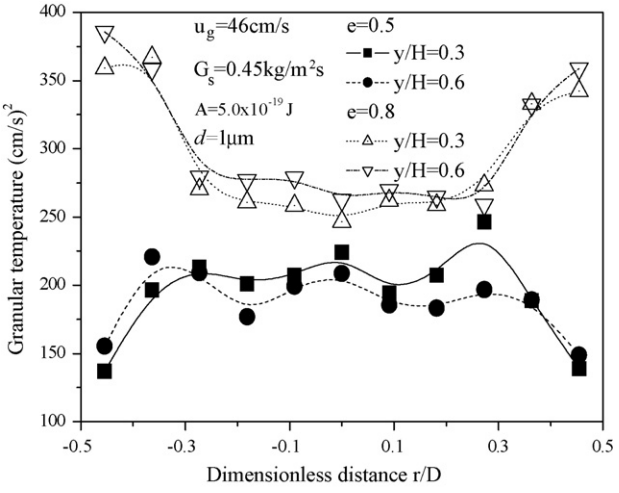

Fig. 21. Profile of standard deviation σ_y of with different collisional parameters.

coefficient of restitution, higher particles concentrations are obtained. Simulations indicated that more agglomerates are formed at low coefficients of restitution in the riser. Uniform distribution of concentration of particles could be obtained at higher restitution coefficients.

Fig. 21 shows the distribution of granular temperature of particles at two different restitution coefficients at the superficial gas velocity and solid mass flux of 46.0 cm/s and 0.45 $kg\,m^{-2}\,s^{-1}$, respectively. The granular temperature increases with the increase of restitution coefficient since the less energy dissipation during collision of particles. These simulations indicate that the coefficient of restitution of particles has a significant effect on the distributions of particle concentration in being a key factor controlling the kinetic energy and hence the dispersion of particles.

4. Conclusions

Computer simulations have been used to investigate flow behavior of micro-particles with interparticle van der Waals forces following Hamaker theory. The dynamic equation of motion for each individual simulated particle of a representative sample is solved by means of the direct simulation Monte Carlo method. The distributions of instantaneous velocity and concentration of these chosen particles in the riser were analyzed and the distributions of averaged concentration and velocity of particles were subsequently obtained. From these results, the particle granular temperature and collisional frequency were predicted. It was found that the computed frequencies of particle collisions at high concentrations significantly depart from the predictions using the kinetic theory of non-cohesive particles, being in agreement only at very low concentration of particles. From an analysis of the particle velocity fluctuations, an anisotropy of the velocity fluctuation of micro-particles exists due to gas–particle interaction and particle collisions. Hence, we observed that the so-called "particle turbulence" is far from being isotropic. We also note, that by discretizing and tracking individual particle trajectories, we gain substantial insight to the collisional and agglomerational processes that enter in solids fluid flows.

We stress that the current results are for two-dimensional only, and can therefore only serve to get a qualitative insight into the physical principles underlying the flow behavior of micro-particles. For a true, quantitative comparison with experiments, clearly, full three-dimensional simulations are required. This work will be the subject of future studies. For a further validation of the model the detailed experimental collisional parameters are required. Moreover, in order to allow the application to practical processes, the effects of the liquid bridging force and electrostatic interactions need to be modeled additionally.

Acknowledgements

This work was supported by Natural Science Foundation of China through Grant No. 20606006 and NSFC-Petro China Company Limited under the cooperative Project No. 20490200. We greatly appreciate the collaboration of the French Ministry of the ecological and sustained development in the INERIS program Nanoris.

References

[1] D. Geldart, Types of gas fluidization, Powder Technol. 7 (1973) 285–292.
[2] J. Chaouki, C. Chavarie, D. Klvana, G. Pajonk, Effect of interparticle forces on the hydrodynamic behavior of fluidized aerogels, Powder Technol. 43 (1985) 117–125.
[3] J. Li, K. Kato, A correlation of the elutriation rate constant for adhesion particles (group C particles), Powder Technol. 118 (2001) 209–218.
[4] P. Russo, R.L. Chirone, Massimilla, S. Russo, Influence of the frequency of acoustic waves on sound-assisted fluidization of beds of fine particles, Powder Technol. 82 (1995) 219–230.
[5] Y. Mawateri, T. Koide, Y. Tatermoto, T. Takeshita, K. Noda, Comparison of three vibrational modes (twist, vertical and horizontal) for fluidization of fine particles, Adv. Powder Technol. 12 (2001) 157–168.
[6] C. Nam, R. Pfeffer, R. Dave, S. Sundaresan, Aerated vibrofluidization of silica nanoparticles, AIChE J. 50 (2004) 1776–1785.
[7] C. Zhu, G.L. Liu, Q. Yu, R. Pfeffer, R.N. Davea, C.H. Nam, Sound assisted fluidization of nanoparticle agglomerates, Powder Technol. 141 (2004) 119–123.
[8] T. Mikami, H. Kamiya, M. Horio, Numerical simulation of cohesive powder behavior in a fluidized bed, Chem. Eng. Sci. 53 (1998) 1927–1940.
[9] E. Helland, R. Occelli, L. Tadrist, Numerical study of cohesive powders in a dense fluidized bed, Comput. Fluid Mech. 327 (1999) 1397–1403.
[10] M.J. Rhodes, X.S. Wang, M. Nquyen, P. Stewart, K. Liffman, Use of discrete element method simulation in studying fluidization characteristics: influence of interparticle force, Chem. Eng. Sci. 56 (2001) 69–76.
[11] K. Kuwagi, M. Horio, A numerical study on agglomerate formation in a fluidized bed of fine cohesive particles, Chem. Eng. Sci. 57 (2002) 4737–4744.
[12] M. Ye, M.A. van Der Hoef, J.A.M. Kuipers, A numerical study of fluidization behavior of Geldart A particles using a discrete particle model, Powder Technol. 139 (2004) 129–139.
[13] C.A. Ho, M. Sommerfeld, Modelling of micro-particle agglomeration in turbulent flows, Chem. Eng. Sci. 57 (2002) 3073–3084.
[14] D. Gidaspow, Multiphase Flow and Fluidization: Continuum and Kinetic Theory Descriptions, Academic Press, Boston, 1994.
[15] L. Huilin, W. Shuyan, Z. Yunhua, Y. Liu, D. Gidaspowb, J. Ding, Prediction of particle motion in a two-dimensional bubbling fluidized bed using discrete hard-sphere model, Chem. Eng. Sci. 60 (2005) 3217–3231.
[16] J.W. Deardorff, On the magnitude of the subgrid scale eddy coefficient, J. Comput. Phys. 7 (1971) 120–133.
[17] B.P.B. Hoomans, J.A.M. Kuipers, W.J. Briels, W.P.M. van Swaaij, Discrete particle simulation of bubble and slug formation in a two-dimensional gas-fluidized bed: a hard-sphere approach, Chem. Eng. Sci. 51 (1996) 99–118.
[18] Z. Haosheng, G. Flamant, D. Gauthier, DEM-LES of coal combustion in a bubbling fluidized bed. Part I. Gas–particle turbulent flow structure, Chem. Eng. Sci. 59 (2004) 4193–4203.
[19] B. Chu, Molecular Forces, Wiley, New York, 1967.
[20] A.F. Fortes, P. Caldas, J.V. Gallo, Particle aggregation and the van der Waals forces in gas–solids fluidization, Powder Technol. 98 (1998) 201–208.
[21] J.P.K. Seville, C.D. Willett, P.C. Knight, Interparticle forces in fluidization: a review, Powder Technol. 113 (2000) 261–268.
[22] G.A. Bird, Molecular Gas Dynamics and the Direct Simulation of Gas Flows, Clarendon Press, Oxford, 1994.
[23] Y. Tsuji, T. Tanaka, S. Yonemura, Cluster patterns in circulating fluidized beds predicted by numerical simulation (discrete particle model versus two-fluid model), Powder Technol. 95 (1998) 254–264.
[24] S. Yuu, N. Hiroyasu, U. Toshihiko, Numerical simulation of air and particle motions in group-B particle turbulent fluidized bed, Powder Technol. 118 (2001) 32–44.
[25] W. Shuyan, L. Huanpeng, L. Huilin, L. Wentie, J. Ding, L. Wei, Flow behavior of clusters in a riser simulated by direct simulation Monte Carlo method, Chem. Eng. J. 106 (2005) 197–211.

[26] Y. Iwadate, M. Horio, Prediction of agglomerate sizes in bubbling fluidized beds of group C powders, Powder Technol. 100 (1998) 223–236.
[27] H. Kim, H. Arastoopour, Extension of kinetic theory to cohesive particle flow, Powder Technol. 122 (2002) 83–94.
[28] L. Huilin, D. Gidaspow, J. Bouillard, L. Wentie, Hydrodynamic simulation of gas–solid flow in a riser using kinetic theory of granular flow, Chem. Eng. J. 95 (2003) 1–13.
[29] L. Huilin, S. Zhiheng, J. Ding, L. Xiang, L. Huanpeng, Numerical simulation of bubble and particles motions in a bubbling fluidized bed using direct simulation Monte-Carlo method, Powder Technol. 169 (2006) 159–171.
[30] S.V. Patankar, Numerical Heat Transfer and Fluid Flow, McGraw-Hill, 1980.
[31] D. Gidaspow, L. Huilin, Equation of state and radial distribution function of FCC particles in a CFB, AIChE J. 44 (1998) 279–293.
[32] A.K. Sharma, K. Tuzla, J. Matsen, J.C. Chen, Parametric effects of particle size and gas velocity on cluster characteristics in fast fluidized beds, Powder Technol. 111 (2000) 114–122.
[33] H. Li, R. Hong, Z. Wang, Fluidizing ultrafine powders with circulating fluidized bed, Chem. Eng. Sci. 54 (1999) 5609–5615.
[34] H.C. Hamaker, London-van der Waals attraction between spherical particles, Physica 4 (1937) 1058–1072.
[35] J. Israelachvili, Intermolecular and Surface Forces, 2nd ed., Academic Press, New York, 1992.
[36] E.M. Lifshitz, The theory of molecular attractive forces between solid bodies, J. Exp. Theor. Phys. 29 (1955) 83–94.